Springer

KSME

Journal of Mechanical Science and Technology 27 (8) (2013) 2477~2486
www.springerlink.com/content/1738-494x
DOI 10.1007/s12206-013-0633-6

Study of an adaptive fuzzy algorithm to control a rectangular-shaped unmanned surveillance flying car †

Kuktae Kim, Kyoil Hwang and Hoonmo Kim*

School of Mechanical Engineering, Sungkyunkwan University, Suwon, 440-746, Korea

(Manuscript Received March 20, 2012; Revised February 1, 2013; Accepted April 12, 2013)

Abstract

In this paper, we propose the concept of the rectangular-shaped unmanned surveillance flying car (RSUSFC), whose design is based on vehicles driven on the road. This RSUSFC offers driving and flying performance as an initial concept of a ground and aerial car. This RSUSFC is built around the previous quad rotor configuration because the quad rotor platform has significant advantages such as construction and maintenance simplicity, hovering ability, and vertical take-off and landing. Traditional quad rotor vehicles are square-shaped and move in the direction of the vertex. However, the RSUSFC moves in the direction of the one side of a rectangle like a traditional car to enhance driving performance. The dynamic modeling of the RSUFC is verified by analysis and simulation. Use of an adaptive fuzzy controller, which is very effective in a complex and nonlinear system, is suggested to stabilize the RSUSFC and is validated by MATLAB simulation.

Keywords: Adaptive fuzzy control; Nonlinear control; Rectangular-shaped unmanned surveillance flying car; Simulation

1. Introduction

Cars have provided us with convenience, such as shortened travel time in our daily lives, but they have also become a source of inconvenience such as traffic jams due to their dramatic increase in number and their geographical limitations. Airplanes have provided us with more convenience, allowing us to move more quickly from here to there with no geographical limitations. However, airplanes have temporal and spatial restrictions, requiring us to travel at specific times to specific places. Scientists have tried to overcome these inconveniences of human inventions. Ultimately, they have found a better way to make our lives more convenient by changing the way we think about the modes of transportation, providing us with a hybrid of a car and an airplane, the flying car.

Scientists at the Moller, a flying car research company, have invented a sky car that is capable of vertical takeoffs and landings [1]. Also, other scientists at Massachusetts Institute of Technology, who founded a company called Terrafugia, have advanced their promising research of the flying car as a better future transportation system [2]. They successfully completed an aeronautical test and are working to turn their new technology into a commercial business. However, both of these flying cars demonstrate poor driving performance because their designs are based on airplanes. In-depth evaluation leads to the conclusion that driving performance is the most important aspect of a flying car since a driver spends most of his time driving on the ground. For these reasons, we propose a rectangular-shaped flying car based on vehicles, not aircrafts, namely the rectangular shaped unmanned surveillance flying car (RSUSFC).

As small surveillance aerial vehicles, fixed wing aircrafts have limited maneuverability and a conventional helicopter is dynamically and structurally complex, expensive, and difficult to control. To solve these kinds of problems, quad rotor vehicles have been proposed. Quad rotor vehicles were first developed in 1922, and their first known successful hover was demonstrated in October of that year [3]. Since then, quad rotor vehicles have been studied extensively [4-13]. S. Bouabdallah et al. presented the design and control of an indoor micro quad rotor [4]. G. Hoffmann et al. developed multi-agent test beds and controlled the quad rotor vehicle using sliding control and the linear quadratic regulator (LQR) technique [5, 6]. However, LQR control has a disadvantage in that it is applicable for linear systems only. Thus, the slow speed of the quad rotor vehicle has to be assumed as in the hovering or the indoor condition so that the vehicle can be approximated as a linear system. However, in the real world, the speed of quad rotor vehicle is high and a gust of wind can negatively influence on its motion. Therefore, LQR control is not effecttive on high speed system such as flying car.

*Corresponding author. Tel.: +82 31 290 7500, Fax.: +82 31 290 7666
E-mail address: kimhm@me.skku.ac.kr
† Recommended by Associate Editor Yang Shi

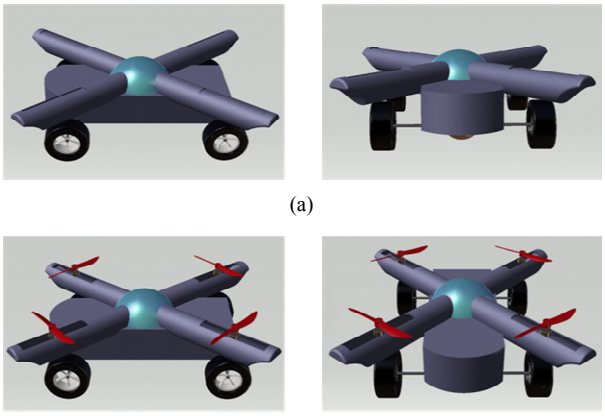

Fig. 1. Concept design of the rectangular-shaped unmanned surveillance flying car: (a) driving; (b) flying.

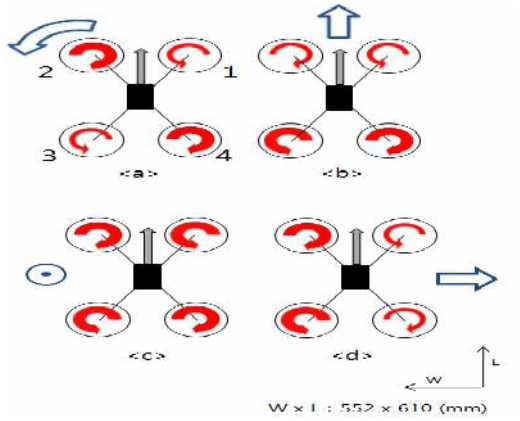

Fig. 2. Description of rectangular-shaped unmanned surveillance flying: (a) yawing control; (b) pitching control; (c) thrust control; (d) rolling control.

D. W. Lee et al. compared feedback linearization to an adaptive sliding mode control for quad rotor vehicles and showed that it worked better under noisy conditions [9]. Sliding control basically converts a complex n^{th} order system into a simple system by removing the higher orders using feedback input. A sliding surface that satisfies the sliding condition must first be defined. If the trajectory is placed outside the surface, the controller makes the system converge to the surface. However, sliding control is only available in a parametrically uncertain model and has a chattering problem because it is a type of switching control.

To realize a robust control without these kinds of problems, adaptive fuzzy control is presented in this paper. An adaptive fuzzy algorithm is a type of robust control that changes the fuzzy rule based on the environmental condition, so it can be used even in unpredictable situations and in those situations with parameters that affect the input variables [14, 16].

The rest of the article is organized as follows. The second section describes the RSUSFC design concept. The third section describes the RSUSFC configuration. The fourth section presents the RSUSFC dynamics. The fifth section shows the simulation results of the RSUSFC dynamics. The adaptive fuzzy control for RSUSFC is represented in the sixth section. The seventh section presents the simulation results of the adaptive fuzzy control. And finally, the last section provides the conclusion and proposes plans for future work.

2. Design concept of the RSUSFC

A design concept of the RSUSFC is represented in Fig. 1. Because we consider the driving performance of quad rotor vehicles is more important than the flying, a rectangular shape is proposed instead of a square shape. The RSUSFC has more advantages than a square counterpart for the same mass and material, such as decreased resistance force during driving because of reduced cross-sectional area, improved comfort during driving due to a lesser vertical disturbance effect on the body and tolerance against pitching disturbances. However, RSUSFC also has the disadvantages of lateral motion during driving and rolling disturbance during flying. Based on the best length-to-width ratio that is not too detrimental to either driving or flying, a rectangular-shaped vehicle seems more reasonable for enhanced driving performance. A RSUSFC consists of four rotors placed at the four corners of a rectangular-shaped body. Upon driving (Fig. 1(a)), the RSUSFC hides the rotors within the shafts to reduce the resistance force, and upon flying (Fig. 1(b)), the rotors are taken out of the shafts. In this paper, we focus on flying control only because flying is more critical than driving.

3. RSUSFC configuration

Most quad rotor vehicles are square-shaped with facing rotors that rotate in the same direction and move in the direction of the vertex.4-9 However, Altug et al. represented a quad rotor vehicle that moves in the direction of the one side of rectangle such as cars, 10 and this is the way we represent RSUSFC motion in this paper. Fig. 2 represents the motion description of RSUSFC, where the arrow width is proportional to the propeller rotational speed. The length and width of RSUSFC are assumed to be 610 mm and 552 mm, respectively. One pair of diagonally opposite rotors rotates clockwise, while the other pair rotates counterclockwise. This configuration obviates several moments from each rotor and allows for easy control.

All maneuvers can be performed by varying the speed of each rotor. Fig. 2(a) shows the yawing control. Yawing is performed when the speeds of rotors 1 and 3are increased and the speeds of rotors 2 and 4 are decreased (or vice versa). Pitching is performed when the speeds of rotors 1 and 2 are decreased and the speeds of the other rotors are increased, as shown in Fig. 2(b). Simultaneously increasing or decreasing the speeds of the four rotors generates vertical motion as shown in Fig. 2(c). Rolling motion (Fig. 2(d)) occurs when the

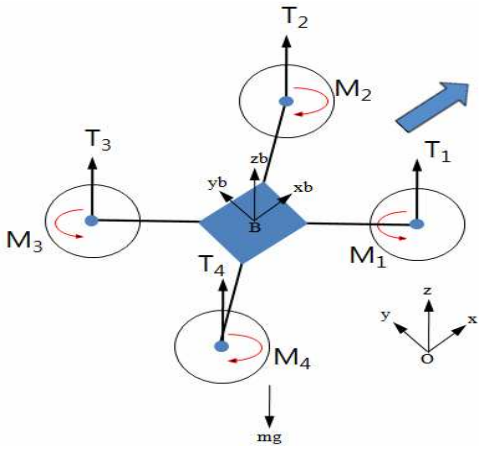

Fig. 3. Free body diagram of rectangular-shaped unmanned surveillance flying car.

speeds of rotors 1 and 4 are increased (or decreased) and the speeds of rotors 2 and 3 are decreased (or increased).

4. Dynamics of RSUSFC

Fig. 3 represents the free body diagram of RSUSFC. Traditional quad rotor vehicles are square, but our RSUSFC is rectangular. The dynamic equation of RSUSFC is presented in this section. T_i is the thrust of each rotor, M_i is the moment of each rotor, and m is the mass of RSUSFC. The body fixed frame is assumed to be located at the center of gravity of the RSUSFC, where the z-axis is pointing upward. This body axis is related to the inertial frame by the position vector (x,y,z) and three Euler angles (θ,ψ,φ), representing pitch, roll, and yaw, respectively. The ZYX-Euler angle representation given in Eq. (1) is chosen to represent the rotations [15].

$$R=\begin{pmatrix} c_\phi c_\theta & c_\phi s_\theta s_\psi - s_\phi c_\psi & c_\phi s_\theta c_\psi + s_\phi s_\psi \\ s_\phi c_\theta & s_\phi s_\theta s_\psi + c_\phi c_\psi & s_\phi s_\theta c_\psi - c_\phi s_\psi \\ -s_\theta & c_\phi s_\psi & c_\theta c_\psi \end{pmatrix} \tag{1}$$

where c_θ and s_θ represent $\cos\theta$ and $\sin\theta$, respectively. Each rotor produces both thrusts and moments. There are four input forces by the four rotors and six output states. The rotation direction of two of the rotors is clockwise, while the other two of them are counterclockwise, so the moments of the RSUSFC are balanced and the desired yaw motions are produced by adjusting the speed of each rotor. The equation of motion of RSUSFC can be represented using the following equations:

$$\ddot{x}=\frac{(\sum_{i=1}^{4}T_i)(\cos\phi\sin\theta\cos\psi+\sin\phi\sin\psi-D_1)}{m}$$

$$\ddot{y}=\frac{(\sum_{i=1}^{4}T_i)(\sin\phi\sin\theta\cos\psi-\cos\phi\sin\psi-D_2)}{m}$$

Table 1. Symbols and their values.

Symbol	Value	Symbol	Value
l_1	0.305(m)	J_1	0.55(kg·m^2)
l_2	0.276(m)	J_2	0.5(kg·m^2)
M	2(kg)	J_3	0.5(kg·m^2)

Table 2. Figures and values of each symbol.

Figure	Tilting angle(°)	T_1(kgf)	T_2(kgf)	T_3(kgf)	T_4(kgf)
Fig. 4	0	1	1	1	1
Fig. 5	30	0.5/cos (30°)	0.5/cos (30°)	0.5/cos (30°)	0.5/cos (30°)
Fig. 6	30	0.5/cos (30°)	0.5/cos (30°)	0.5/cos (30°)	0.5/cos (30°)
Fig. 7	0	0.6	0.4	0.6	0.4
Fig. 8	0	0.42	0.42	0.62	0.62
Fig. 9	0	0.4	0.7	0.4	0.7

$$\begin{aligned} \ddot{z} &= \frac{(\sum_{i=1}^{4}T_i)(\cos\phi\cos\psi-mg-D_3)}{m} \\ \ddot{\theta} &= l_1(-T_1-T_2+T_3+T_4-D_4)/J_1 \\ \ddot{\psi} &= l_2(-T_1+T_2+T_3-T_4-D_5)/J_2 \\ \ddot{\phi} &= (M_1-M_2+M_3-M_4-D_6)/J_3 \end{aligned} \tag{2}$$

where D_i is the resistance force, J_i is the moment of inertia, l_1 is the length of the body from the body center of the RSUSFC, and l_2 is the width of the body from the body center of the RSUSFC.

5. Verification of RSUSFC dynamics

The design concept of RSUSFC was presented in section 2 and the dynamic equations were presented in section 4. In this section, the validity of the dynamic equations is checked. Figs. 4-9 represent $\dot{x}$ versus time, x versus time in vertical motion, $\dot{v}$ versus time, y versus time, $\dot{z}$ versus time, z versus time, $\dot{\theta}$ versus time, θ versus time in forward motion, $\dot{\psi}$ versus time, ψ versus time, $\dot{\phi}$ versus time, and ϕ versus time in lateral motion, respectively. MATLAB was used for the simulation. The parameters assumed in the simulation are shown in Table 1, and thrusts and tilting angles in each figure are represented in Table 2.

Fig. 4 shows vertical motion of flying car. We input 1kgf to each rotor. $x, y, \dot{x}, \dot{y}, \theta, \psi, \phi, \dot{\theta}, \dot{\psi}$ and $\dot{\phi}$ are zero. $\dot{z}$ is increased first and converges to about 17 km/s under drag force. z is linearly increased after 3 seconds. For forward motion shown in Fig. 5, the RSUSFC body was tilted 30° forward and 0.5/cos(30°) kgf was applied to cancel out the gravity force. $\dot{x}$ is increased first and converges to about 13 km/s due to drag force, and x continuously increases. Fig. 6 represents the side motion, and the principle of the motion is

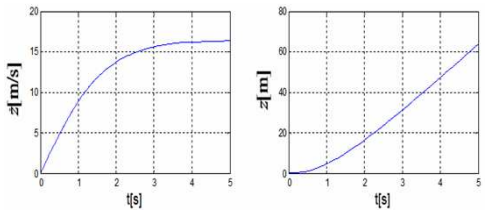

Fig. 4. Vertical motion: (T1, T2, T3, T4) = (1, 1, 1, 1).

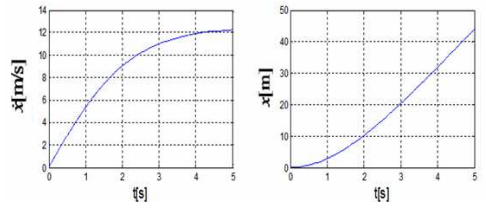

Fig. 5. Forward motion (tilting angle, 30°): (T1, T2, T3, T4) = (0.5/cos (30°), 0.5/cos (30°), 0.5/cos (30°), 0.5/cos (30°)).

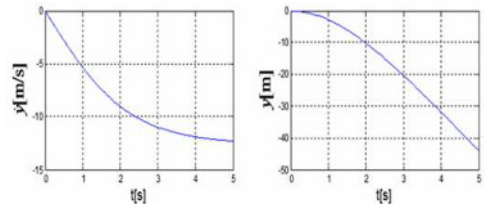

Fig. 6. Lateral motion (tilting angle, 30°): (T1, T2, T3, T4) = (0.5/cos (30°), 0.5/cos (30°), 0.5/cos (30°), 0.5/cos (30°)).

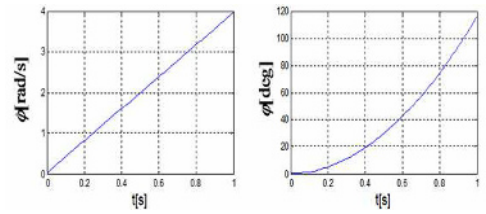

Fig. 7. Yawing motion; (T1, T2, T3, T4) = (0.6, 0.4, 0.6, 0.4).

similar to the forward motion shown in Fig. 5. Fig. 7 shows the yawing motion. We input 0.6 kgffor T1, T3 and 0.4 kgffor T2, T4 to counterbalance the gravity force, pitching, and rolling motion. Fig. 8 displays the pitching motion, for which we input 0.42 kgffor T1, T2 and 0.62 kgffor T3, T4. Note that not only θ and $\dot{\theta}$ but also $x, z, \dot{x}$, and $\dot{z}$ are changed because the dynamic equations of $\ddot{x}$ and $\ddot{z}$ are coupled with θ. Therefore, the proper input value that will not greatly affect the z and x motions should be found. In Fig. 8, when we change θ from 0° to 30°, x from 0 m to 0.2 m, and z from 0m to 0.2 m, respectively. Fig. 9 shows the rolling motion control, which is similar to the pitching motion control shown in Fig. 8. The dynamics of the RSUSFC are well derived from the concept model; as expected, RSUSFC is more robust in pitching motion than in rolling motion because of its rectangular shape.

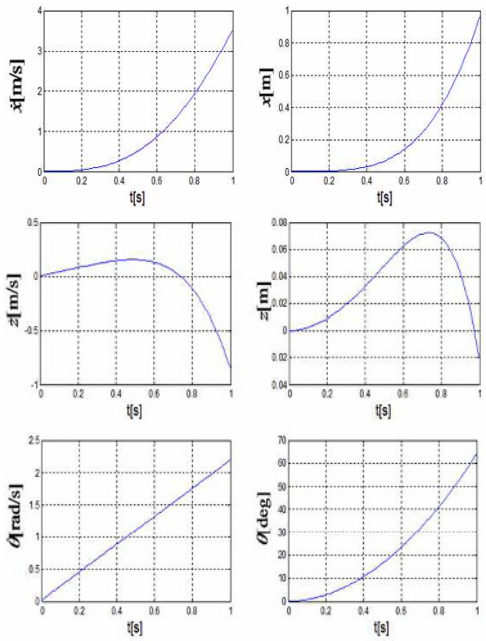

Fig. 8. Pitching motion: (T1, T2, T3, T4) = (0.42, 0.42, 0.62, 0.62).

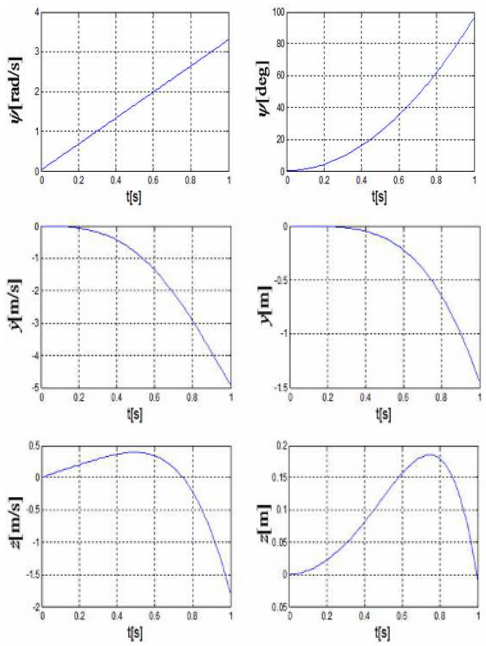

Fig. 9. Rolling motion: (T1, T2, T3, T4) = (0.4, 0.7, 0.4, 0.7).

6. Control of a RSUSFC

In this section, an adaptive fuzzy control strategy is suggested to stabilize the RSUSFC in the presence of unknown dynamic parameters. We use the direct adaptive fuzzy control, in which the parameters are directly adjusted to reduce some of the norm of the output error between the actual model and the reference model, and the first type adaptive fuzzy controller, in which fuzzy logic systems have linear adjustable parameters. Thus, a fuzzy logic system looks like this [16]:

$$f(x)=\sum_{l=1}^{M}\theta_l\xi_l(x) \\ =\underline{\theta}^T\underline{\xi}(\underline{x}) \tag{3}$$

where $\underline{\theta}=(\theta_1,\cdots,\theta_M)^T$ and $\underline{\xi}(\underline{x})=(\underline{\xi}_1(\underline{x}),\cdots,\underline{\xi}_M(\underline{x}))^T$. $\xi_l(\underline{x})$ is the fuzzy basis function defined here [16]:

$$\xi_l(\underline{x})=\frac{\prod_{i=1}^{n}\mu_{F_i^l}(x_i)}{\sum_{l=1}^{M}\prod_{i=1}^{n}\mu_{F_i^l}(x_i)}. \tag{4}$$

6.1 Control objectives

Consider the system [16]

$$x^{(n)}=f(x,\dot{x},\cdots,x^{(n-1)})+bu,\quad y=x \tag{5}$$

where f is an unknown function; b is a positive unknown constant; and $u\in R$ and $y=x$ are the system input and output, respectively. We assume that it is possible to measure the state vector $\underline{x}=(x,\dot{x},\cdots,x^{(n-1)})^T$. The control objective is to force y to follow a given bounded reference signal, $y_m(t)$, under the constraint that all signals involved must be bounded.

6.2 Supervisory control

Suppose that control u is the summation of basic control $u_c(\underline{x}\,|\,\underline{\theta})$ and supervisory control $u_s(\underline{x})$ such as [16]:

$$u=u_c(\underline{x}\,|\,\underline{\theta})+u_s(\underline{x}). \tag{6}$$

If we know $f(\underline{x})$ and b, then [16]

$$u^*=\frac{1}{b}[-f+y_m^{(n)}+\underline{k}^T\underline{e}] \tag{7}$$

will force e to converge to zero, where $\underline{e}=(e,\dot{e},\cdots,e^{(n-1)})^T$ and $\underline{k}=(k_n,k_{n-1},\cdots,k_1)^T$ such that all roots of $s^n+k_1s^{n-1}+\cdots+k_n=0$ are in the left half-plane. After some manipulation, we obtain the error equation governing the closed-loop system as [16]:

$$\dot{\underline{e}}=\Lambda_c\underline{e}+\underline{b}_c[u^*-u_c(\underline{x}\,|\,\underline{\theta})-u_s(\underline{x})] \tag{8}$$

where [16]

$$\Lambda_c=\begin{bmatrix}0&1&0&0&\cdots&0&0\\0&0&1&0&\cdots&0&0\\\cdots&\cdots&\cdots&\cdots&\cdots&\cdots&\cdots\\0&0&0&0&\cdots&0&1\\-k_n&-k_{n-1}&\cdots&\cdots&\cdots&\cdots&-k_1\end{bmatrix},\ \underline{b}_c=\begin{bmatrix}0\\\cdots\\0\\b\end{bmatrix}. \tag{9}$$

Define the Lyapunov function candidate [16]:

$$V_e=\frac{1}{2}\underline{e}^Tp\underline{e} \tag{10}$$

where p is a symmetric positive definite matrix satisfying [16]:

$$\Lambda_c^TP+P\Lambda_c=-Q. \tag{11}$$

Using Eqs. (11) and (8), we have [16]

$$\dot{V}_e=-\frac{1}{2}\underline{e}^TQ\underline{e}+\underline{e}^TP\underline{b}_c[u^*-u_c(\underline{x}\,|\,\underline{\theta})-u_s(\underline{x})] \\ \le-\frac{1}{2}\underline{e}^TQ\underline{e}+|\,\underline{e}^TP\underline{b}_c\,|\,(|\,u^*\,|+|\,u_c\,|)-\frac{1}{2}\underline{e}^TP\underline{b}_cu_s. \tag{12}$$

Assumption: We can determine a function $f^U(\underline{x})$ and a constant b_L such that $|\,f(\underline{x})\,|\le f^U(\underline{x})$ and $0\le b_L\le b$.

We then construct the supervisory control $u_s(\underline{x})$ as [16]:

$$u_s(\underline{x})=I_1^*\,\mathrm{sgn}(\underline{e}^TP\underline{b}_c)[|\,u_c\,|+\frac{1}{b_L}(f^u+|\,y_m^{(n)}\,|+|\,\underline{k}^T\underline{e}\,|)] \tag{13}$$

where $I_1^*=1$ if $V_e>\overline{V}$ and $I_1^*=0$ if $V_e\le\overline{V}$. Replacing Eq. (12) with Eqs. (13) and (7) and considering the $I_1^*=1$ case, we have [16]

$$\dot{V}_e\le-\frac{1}{2}\underline{e}^TQ\underline{e}+|\,\underline{e}^TP\underline{b}_c\,|[\frac{1}{b}(|\,f\,|+|\,y_m^{(n)}\,|+|\,\underline{k}^T\underline{e}\,|) \\ +|\,u_c\,|-|\,u_c\,|-\frac{1}{b_L}(f^U+|\,y_m^{(n)}\,|+|\,\underline{k}^T\underline{e}\,|)] \\ \le-\frac{1}{2}\underline{e}^TQ\underline{e}\le0. \tag{14}$$

Therefore, using the supervisory control u_s, we always have $V_e\le\overline{V}$. The boundedness of V_e implies the boundednessof $\underline{e}$, which in turn implies the boundedness of $\underline{x}$ because $P>0$.

6.3 Online adaption law

Define the optimal parameter vector as [16]:

$$\underline{\theta}^*=\arg\min_{|\underline{\theta}|\le M_\theta}[\sup_{|\underline{x}|\le M_x}|\,u_c(\underline{x}\,|\,\underline{\theta})\,|-u^*] \tag{15}$$

and the minimum approximation error as [16]

$$w\equiv u_c(\underline{x}\,|\,\underline{\theta}^*)-u^*. \tag{16}$$

Now the Eq. (8) can be rewritten as [16]

$$\dot{\underline{e}}=\Lambda_c\underline{e}+\underline{b}_c[u_c(\underline{x}\,|\,\underline{\theta}^*)-u_c(\underline{x}\,|\,\underline{\theta})]-\underline{b}_cu_s(\underline{x})-\underline{b}_cw. \tag{17}$$

If we choose $u_c(\underline{x}\,|\,\underline{\theta})$ in the form of Eq. (4), then Eq. (17)

becomes [16]

$$\dot{\underline{e}} = \Lambda_c \underline{e} + \underline{b}\underline{\phi}^T \underline{\xi}(\underline{x}) - \underline{b}_c u_s(\underline{x}) - \underline{b}_c w \tag{18}$$

where $\phi \equiv \underline{\theta}^* - \underline{\theta}$ and $\underline{\xi}(\underline{x})$ is the fuzzy basis function. Let's define the Lyapunov function as [16]

$$V_e = \frac{1}{2}\underline{e}^T P \underline{e} + \frac{b}{2\gamma}\underline{\phi}^T \underline{\phi}. \tag{19}$$

We obtain Eq. (20) using Eqs. (18) and (11) [16]

$$\dot{V}_e = -\frac{1}{2}\underline{e}^T Q \underline{e} + \underline{e}^T P \underline{b}_c (\underline{\phi}^T \underline{\xi}(\underline{x}) - u_s - w) + \frac{b}{\gamma}\underline{\phi}^T \dot{\underline{\phi}} \tag{20}$$

where $\underline{P}_n$ is the last column of p. Then from Eq. (9) we have [16]

$$\underline{e}^T P \underline{b}_c = \underline{e}^T \underline{P}_n \underline{b}_c. \tag{21}$$

Substituting Eq. (21) into Eq. (20), we have [16]

$$\dot{V}_e = -\frac{1}{2}\underline{e}^T Q \underline{e} + \frac{b}{\gamma}\underline{\phi}^T (\gamma \underline{e}^T \underline{p}_n \underline{\xi}(\underline{x}) + \dot{\underline{\phi}}) - \underline{e}^T P \underline{b}_c u_s - \underline{e}^T P \underline{b}_c w. \tag{22}$$

If we choose the adaptive law as follows [16]:

$$\dot{\underline{\theta}} = \gamma \underline{e}^T \underline{p}_n \underline{\xi}(\underline{x}) \tag{23}$$

then Eq. (22) becomes [16]

$$\dot{V} \le -\frac{1}{2}\underline{e}^T Q \underline{e} - \underline{e}^T P \underline{b}_c w. \tag{24}$$

If $w = 0$, we have $\dot{V} \le 0$ because $-\frac{1}{2}\underline{e}^T Q \underline{e} \le 0$. If $w \neq 0$, we can expect that w should be small according to the universal approximation theorem. Therefore, this is the best solution we can attain.

7. Results

7.1 Altitude control

Altitude control is performed in this paper to check the suitability of the adaptive fuzzy controller proposed to control the RSUSFC. In the simulation, the values of the parameters are the same as those in Table 1. The initial state is $[x\ y\ z\ \dot{x}\ \dot{y}\ \dot{z}\ \theta\ \psi\ \phi\ \dot{\theta}\ \dot{\psi}\ \dot{\phi}]^T = [0\ 0\ 0\ 0\ 0\ 0\ 0\ 0\ 0\ 0\ 0\ 0]^T$. The control objective is to make RSUSFC track the reference input, z = 1 m. We define six fuzzy sets over the interval [–1, 1] with labels NB, NM, NS, Zero, PS, PM, and PB, and membership functions $\mu_{NB} = \exp(-25\times(x+1)^2)$, $\mu_{NM} = \exp(-25\times(x+0.6666)^2)$, $\mu_{NS} = \exp(-25\times(x+0.3334)^2)$, $\mu_{Zero} = \exp(-25\times(x)^2)$, $\mu_{PS} = \exp(-25\times(x-0.3334)^2)$, $\mu_{PM} = \exp(-25\times(x-0.6666)^2)$, and $\mu_{PB} = \exp(-25\times(x-1)^2)$ as shown in Fig. 10. The fuzzy rule table is represented in Table 3. From section 6, the control parameters are chosen as follows:

$$\Lambda_c = \begin{bmatrix} 0 & 1 \\ -1 & -2 \end{bmatrix};\ Q = \begin{bmatrix} 10 & 0 \\ 0 & 10 \end{bmatrix};$$

$$P = \begin{bmatrix} 15 & 5 \\ 5 & 5 \end{bmatrix};\ \gamma = 2;\ M_x = 0.2;\ M_\theta = 3;$$

$b_L = 0.5$; and $f^u = -0.3543372 \times \dot{z}^2$.

Table 3. Fuzzy rule table for the altitude control of a rectangular-shaped unmanned surveillance flying car.

		e						
		NB	NM	NS	ZO	PS	PM	PB
e	NB	PB	PB	PB		PB	PS	ZO
	NM	PM	PM	PM		PM	ZO	NS
	NS	PS	PS	PS		PS	NS	NM
	ZO							
	PS	ZO	PS	NS		NS	NS	NS
	PM	NS	ZO	NM		NM	NM	NM
	PB	NM	NS	NB		NB	NB	NB

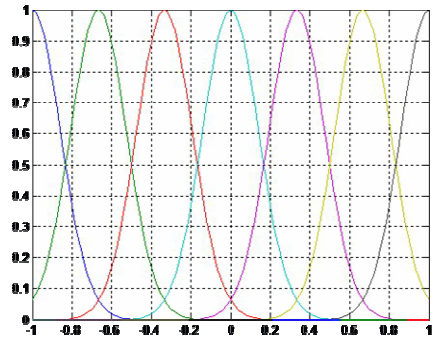

Fig. 10. Fuzzy membership functions defined over the state space for the altitude control of a RSUFC.

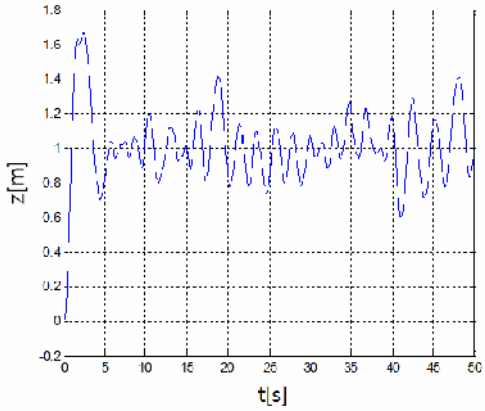

Fig. 11. Altitude control using fuzzy control.

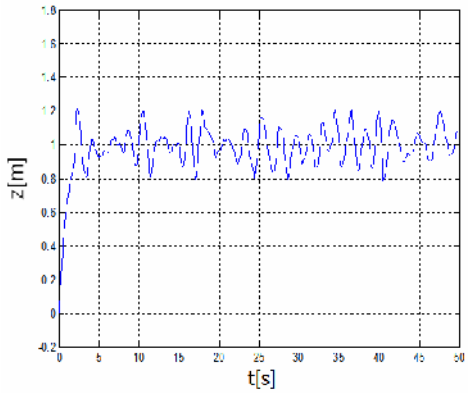

Fig. 12. Altitude control using fuzzy control and supervisor control.

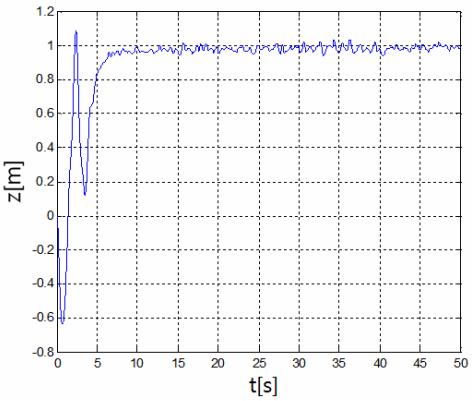

Fig. 13. Altitude control using fuzzy adaptation control.

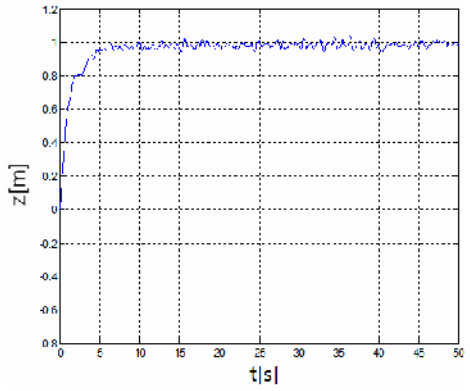

Fig. 14. Altitude control using adaptive fuzzy control.

The results are represented in Figs. 11-14, where RSUSFC moves from 0 m to 1 m in the z direction for 50 seconds. To consider the noise disturbance, we add 5% random noise to each input thrust and to show robust control in a harsh situation such as gusting, we add a maximum 7 N random force in the z direction.

Fig. 11 represents the altitude control using the fuzzy controller. RSUSFC follows the reference input $z = 1$ m; however, the maximum error of z position is 0.65 m at about 2.5 seconds. Altitude control using fuzzy control and supervisor control is represented in Fig. 12. Compared to Fig. 11, the supervisor controller operates when the error passes 0.2 m to prevent the error from exceeding 0.2 m from the reference. Fig. 13 shows the altitude control using the fuzzy adaptation control. It shows that the adaptation method of the fuzzy controller is more stable than traditional fuzzy controller after a few unstable moments in the initial state, up to 5 seconds in this case. Fig. 14 represents the altitude control using the adaptive fuzzy control. From the starting point to about 2.5 seconds, in which the error exceeds 0.2 m, the supervisor controller operates and then the fuzzy adaptation method solely operates. Adaptive fuzzy control is shown to be the most suitable controller for high nonlinear systems such as RSUSFC.

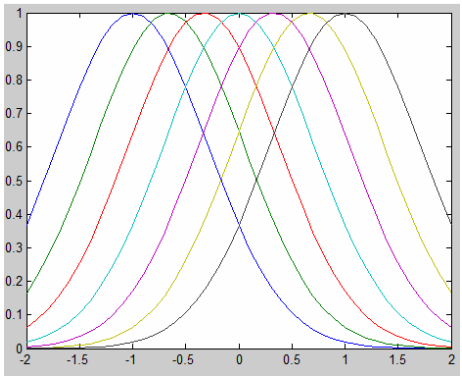

Fig. 15. Fuzzy membership functions for the pitch control of the RSUFC.

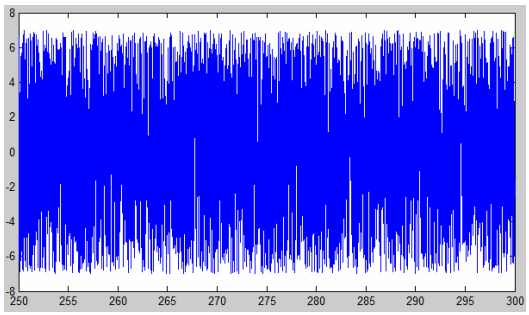

Fig. 16. Maximum 7 N random noise which is added in z direction.

7.2 Motion control

7.2.1 Pitch control

The pitch control of the RSUFC is performed by adaptive fuzzy control. To create pitch motion, we input more torque for T3, T4 than for T1, T2 as shown in Eq. (2). We define six fuzzy sets over the interval $[-1, 1]$ with labels NB, NM, NS, Zero, PS, PM, and PB and membership functions, $\mu_{NB} = \exp(-(x+1)^2)$, $\mu_{NM} = \exp(-(x+0.6666)^2)$, $\mu_{NS} = \exp(-(x+0.3334)^2)$, $\mu_{Zero} = \exp(-(x)^2)$, $\mu_{PS} = \exp(-(x-0.3334)^2)$, $\mu_{PM} = \exp(-(x-0.6666)^2)$, and $\mu_{PB} = \exp(-(x-1)^2)$, are represented in Fig. 15. Table 3 represents fuzzy rule table.

The control objective is to make the RSUFC follow the si-

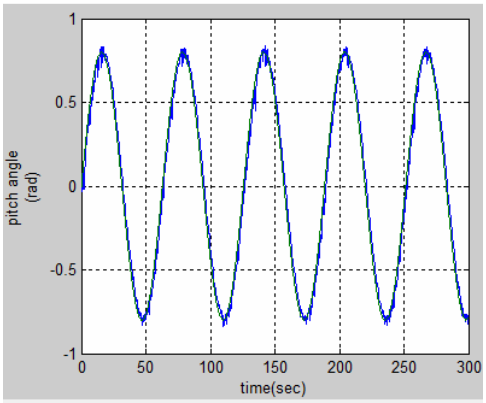

Fig. 17. Pitch control using adaptive fuzzy control.

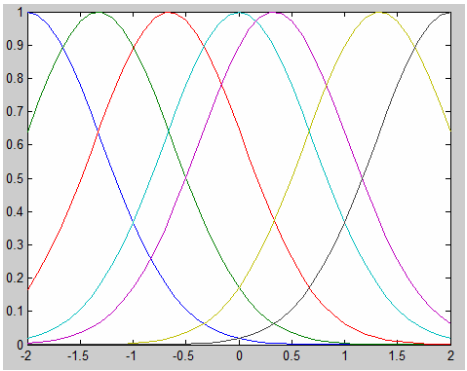

Fig. 18. Fuzzy membership functions for the roll control of the RSUFC.

nusoidal reference input such as Eq. (25).

$$y = 0.8\sin(0.1t)\,. \tag{25}$$

As we did last section, to consider the noise disturbance, we add 5% random noise to each input thrust. To show robust control with uncertainties such as gusting, the maximum 7 N random noise is injected into the system shown in Fig. 16. The pitch control result is shown in Fig. 17. The maximum error is about 5% at peak point such as 20 seconds, 80 seconds, etc. This result demonstrates that adaptive fuzzy control is suitable for high nonlinear situations like those encountered by the RSUSFC.

7.2.2 Roll control

Roll motion control of the RSUSFC is performed using adaptive fuzzy control. We apply different thrust between T2, T3 and T1, T2 to develop the roll variation. We define six fuzzy sets over the interval $[-1,\ 1]$ with labels NB, NM, NS, Zero, PS, PM, and PB and membership functions, $\mu_{NB} = \exp(-(x+2)^2)$, $\mu_{NM} = \exp(-(x+1.33)^2)$, $\mu_{NS} = \exp(-(x+0.66)^2)$, $\mu_{Zero} = \exp(-(x)^2)$, $\mu_{PS} = \exp(-(x-0.66)^2)$, $\mu_{PM} = \exp(-(x-1.33)^2)$, and $\mu_{PB} = \exp(-(x-2)^2)$, are represented in Fig. 18. The fuzzy rule table is represented in Table 3.

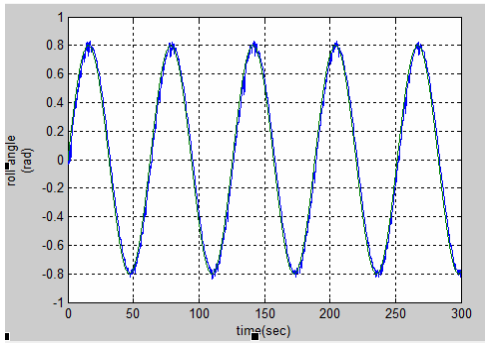

Fig. 19. Roll control using adaptive fuzzy control.

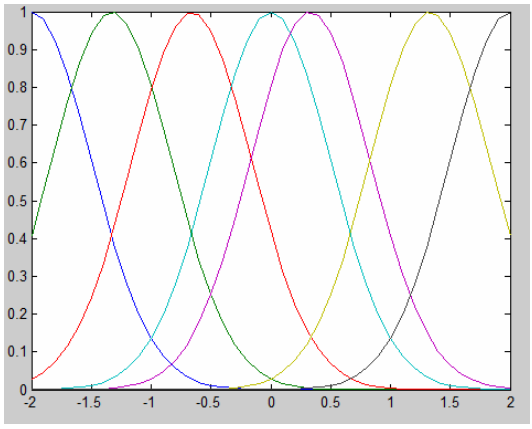

Fig. 20. Fuzzy membership functions for the yaw.

The reference input and noise are the same as pitch control, and the result is shown in Fig. 19. The maximum error is about 5% at peak point from the reference, and the result is similar to that of pitch control. Adaptive fuzzy control is a suitable controller as well.

7.2.3 Yaw control

Using adaptive fuzzy control, we perform yaw control. The control input is different between M1, M3 and M2, M4 input thrusts to create the yaw motion. Six fuzzy sets are defined over the interval $[-1,\ 1]$ with labels NB, NM, NS, Zero, PS, PM, and PB and membership functions, $\mu_{NB} = \exp(-0.9(x+2)^2)$, $\mu_{NM} = \exp(-0.9(x+1.33)^2)$, $\mu_{NS} = \exp(-0.9(x+0.66)^2)$, $\mu_{Zero} = \exp(-0.9(x)^2)$, $\mu_{PS} = \exp(-(x-0.66)^2)$, $\mu_{PM} = \exp(-0.9(x-1.33)^2)$, and $\mu_{PB} = \exp(-0.9(x-2)^2)$, are shown in Fig. 20. The fuzzy rule table represented in Table 3 is also used for yaw control.

The reference input and noise are the same as in the previous controls, and the result is shown in Fig. 21. The maximum error is about 5% at peak point, and the result is similar to those of pitch control and roll control. Adaptive fuzzy control is suitable for yaw motion control as well.

8. Conclusion and future work

A three-dimensional concept model and dynamics of an

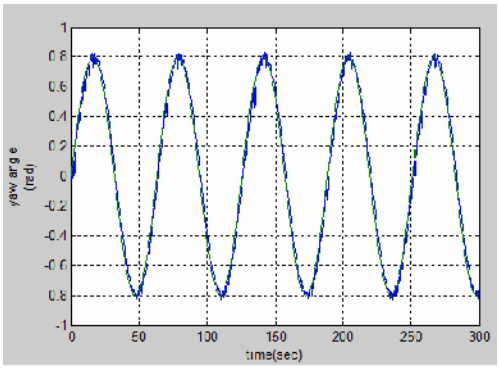

Fig. 21. Yaw control using adaptive fuzzy control.

RSUSFC were presented in this paper. The rectangular shape had some benefits in that the resistance force during driving is decreased because of the reduced cross-sectional area. Driving comfort is improved because the rectangular shape vehicle is less subject to influence on vertical disturbance and has higher tolerance against pitching disturbances. Simulation results of the RSUSFC motion validated its dynamics. In section 6, the use of adaptive fuzzy control as a controller was suggested to overcome the innate highly nonlinear condition of high-speed motions. The adaptive fuzzy algorithm is a type of robust control that can be used even for unpredictable situations with parameters that affect the input variables since it changes the fuzzy rule base according to the environmental condition.

Simulations were then performed to validate the controller using MATLAB Simulink. Hovering control was achieved by fuzzy control, fuzzy control with supervisor, and adaptive fuzzy control. From the simulation results, adaptive fuzzy was more stable and robust than the other control algorithms. Pitch, roll, and yaw controls were implemented using adaptive fuzzy control. The simulation results showed that adaptive fuzzy control is highly effective on RSUSFC motion control.Adaptive fuzzy control is based on the robust fuzzy rule changing theory for unpredictable circumstances or for situations with parameters that affect the input variables, and it is very useful for fast-moving systems such as flying cars.

Our next goal is to conduct an experiment focusing on the flying aspect of RSUSFC. We will then simulate the driving motion of the RSUSFC and conduct driving experiments. A full model of the RSUSFC that focuses on both flying and driving will be introduced by simulation. Finally, a full RSUSFC model will be presented and experiments will be conducted.

Nomenclature

x, y, z : Position vector of RSUSFC
$\dot{x}, \dot{y}, \dot{z}$: Velocity of RSUSFC
$\ddot{x}, \ddot{y}, \ddot{z}$: Acceleration of RSUSFC
θ, ϕ, ψ : Pitch, yaw, roll angle of RSUSFC
$\dot{\theta}, \dot{\phi}, \dot{\psi}$: Angular velocity of RSUSFC
$\ddot{\theta}, \ddot{\phi}, \ddot{\psi}$: Angular acceleration of RSUSFC
D_i : Resistance force
J_i : Moment of inertia
T_i : Thrust of rotor
M_i : Moment of rotor
l_1 : Length of body from body center of RSUSFC
l_2 : Width of body from body center of RSUSFC
m : Mass of RSUSFC
θ_i : Adjustable parameter
$\mu_{F_i^l}$: Membership functions
e : Error of RSUSFC altitude

References

[1] *Skycar*, http://www.moller.com/, Web, 1 Jan. (2013).
[2] *The Transition*, http://www.terrafugia.com/, Web, 1 Jan. (2013).
[3] P. Lambermont, *Helicopters and autogyros of the world*, Barnes, New York, USA (1958).
[4] S. Bouabhallah, P. Murrieri and R. Siegwart, Design and control of an indoor micro quadrotor, *Proc. of IEEE International Conference on Robotics and Automation*, 5 (1) (2004) 4393-4398.
[5] G. Hoffmann, D. G. Rajnarayan, S. L. Waslander, D. Dostal, J. S. Jang and C. J. Tomlin, The stanford testbed of autonomous rotorcraft for multi-agent control, *Proc. of AIAA/IEEE Digital Avionics Systems Conference*, 2 (1) (2007) 12.E.4-1-12.E.4-10.
[6] G. M. Hoffmann, H. Huang, S. L. Waslander and C. J. Tomlin, Quadrotor helicopter flight dynamics and control: Theory and experiment, *AIAA Guidance, Navigation, and Control Conference*, 2 (1) (2007) 1670-1689.
[7] P. Castillo, A. Dzul and R. Lozano, Real-time stabilization and tracking of a four-rotor mini rotorcraft, *IEEE Transactions on Control Systems Technology*, 12 (4) (2004) 510-516.
[8] X. Gong, Z. C. Hou, C. J. Zhao, Y. Bai and Y. T. Tian, Adaptive backstepping sliding mode trajectory tracking control for a quad-rotor, *International Journal of Automation and Computing*, 9 (5) (2012) 555-560.
[9] D. W. Lee, H. J. Kim and S. Sastry, Feedback linearization vs. adaptive sliding mode control for a quadrotor helicopter, *International Journal of Control, Automation and Systems*, 7 (3) (2009) 419-428.
[10] E. Altug, J. P. Ostrowski and C. J. Taylor, Control of a quadrotor helicopter using dual camera visual feedback, *The International Journal of Robotics Research*, 24 (5) (2005) 329-341.
[11] L. R. G. Carrillo, A. Dzul and R. Lozano, Hovering quadrotor control: a comparison of nonlinear controllers using visual feedback, *IEEE Transactions on Aerospace and Electronic Systems*, 48 (4) (2012) 3159-3170.
[12] Y. Naidoo, R. Stopforth and G. Bright, Quad-rotor unmanned aerial vehicle helicopter modelling & control, *International Journal of Advanced Robotic Systems*, 8 (4) (2011) 130-149.
[13] H. Bouadi, M. Bouchoucha and M. Tadjine, Sliding mode control based on backstepping approach for an UAV type-

quadrotor, *World Academy Science, Engineering and Technology*, 26 (1) (2007) 22-27.
[14] L. D. Hanh, K. K. Ahn, N. B. Kha and W. K. Jo, Trajectory control of electro-hydraulic excavator using fuzzy self tuning algorithm with neural network, *Journal of Mechanical Science and Technology*, 23 (1) (2009) 149-160.
[15] J. J. Craig, *Introduction to robotics*, third edition, Prentice Hall, 43-45, New Jersey, USA (2005).
[16] L. X. Wang, *Adaptive fuzzy systems and control*, Prentice Hall, 102-154, New Jersey, USA (1994).

Kuktae Kim received the B.S. and M.S. degree from Sungkyunkwan University in 2008 and 2010, respectively. He currently studies for Ph.D. in Texas A&M University. His research interests include motion and force control, highly nonlinear control, multi-server and multi-client network control.

Kyoil Hwang received his B.S. degree in Mechanical Engineering from Sung kyunkwan University, Korea, in 2000. He then received his M.S. degree from Sungkyunkwan University in 2002. He is a doctor candidate in the Automatic Control Laboratory at Sungkyunkwan University.

Hun Mo Kim received his B.S. degree in Mechanical Engineering from Sung kyunkwan University, Korea, in 1984. He then received his M.S. degree of Aerospace Engineering from University of Michigan, U.S.A.1990. He then received Ph.D. degree in Mechanical Engineering from University of Alabama, U.S.A.1993.He is a professor in the Department of Mechanical Engineering at Sungkyunkwan University.